Enhancing Timer-Based Power Management to Support Delay-Intolerant Uplink Traffic in Infrastructure IEEE 802.11 WLANs

Yi-Hua Zhu, *Senior Member, IEEE*, Shenji Luan, Victor C. M. Leung, *Fellow, IEEE*, and Kaikai Chi, *Member, IEEE*

***Abstract*—Efficient power management of the radio is a critical requirement for the battery-operated portable electronic devices incorporating wireless transceivers to have a longer runtime. The power management function of IEEE 802.11 wireless local area networks (WLANs) allows stations (STAs) to operate in the doze mode to save energy significantly. In this paper, the enhanced timer-based power management (E-TPM) scheme, which supports the applications with delay-intolerant uplink traffic (DIUT), is presented for infrastructure IEEE 802.11 WLANs. With E-TPM, the radio transceiver of the dozing STA is woken up right away when an outgoing frame is generated by the STA so that DIUT is transmitted in a timely manner. In addition, a novel model for stochastic analysis of the E-TPM is developed. Based on this model, the probabilities that an STA is active, idle, or dozing are derived, and the power consumption of the STA, the number of frames buffered at the access point (AP) for the STA operating in doze mode, and the average delay per frame are obtained. These results enable an efficient power management algorithm that optimizes the idle timer and doze duration at the STA so that the doze mode does not result in extra delay in DIUT, and the delay of downlink traffic is controlled within a given bound. Numerical results show that the proposed E-TPM is able to considerably reduce delay with limited available memory space at the AP.**

***Index Terms*—Energy conservation, IEEE 802.11, power management, wireless local area network (WLAN).**

I. Introduction

IEEE 802.11 wireless local area network (WLAN) [1], [2] interfaces, or Wi-Fi, are increasingly being incorporated into multimedia portable electronic devices, which enable them to access the Internet wherever WLAN access points (APs) are located. Most IEEE 802.11 WLANs operate in the infrastructure mode, in which each station (STA) is associated with an AP to access the Internet. The AP and the set of STAs communicating with it form a basic service set, which share a common radio channel using the carrier-sense multiple access with collision avoidance (CSMA/CA) protocol that forms the basis of the distributed coordination function in the IEEE 802.11 standard.

Most STAs are powered by batteries. Hence, it is important to use available battery power efficiently so that the STAs have long runtimes. As the radio transceiver of a WLAN interface has a particularly high power consumption, the IEEE 802.11 standard includes a basic power management (BPM) scheme that allows an STA to switch its transceiver to doze mode (also referred to as sleep mode) to save power. Under BPM, any STA not engaged in active data communication is allowed to sleep after the end of the next beacon frame transmitted by the AP with which the STA is associated.

With power management, after an STA is powered up, it will operate in one of the following modes at any instance: transmitting, receiving, idle, or doze. In the idle mode, the STA is not engaged in any transmitting or receiving activity. After the STA has been idle for a period of time, it may enter the doze mode. In the doze mode, the STA is unable to transmit/receive any frame, but it has very low power consumption. Compared with the other three modes, the power consumption of doze mode is quite small. For instance, the power consumption of the Lucent IEEE 802.11 WaveLan card is 284, 190, 156, and 10 mA for transmitting, receiving, idle, and doze modes, respectively [3]. In addition, the 5004 MP Atheros 4G CM9 802.11a/b/g miniPCI Card, which is provided by the Netgate Company and listed as the top seller up-to-date, consumes 420, 300, 260, and 50 mA when it operates in transmitting, receiving, idle, and doze modes, respectively, when the 802.11a protocol is applied [4]. As a result, most power management schemes aim at maximizing the time when the STA is in doze mode and minimizing the time for the STA to be awake.

When the STA is in doze mode, its associated AP is responsible for buffering data frames destined for the STA. The AP assembles a traffic indication map (TIM) periodically, which is then transmitted in a beacon frame to announce the presence of buffered traffic to STAs operating in doze mode. Meanwhile, the dozing STAs periodically wake up to receive the TIM. They either terminate doze mode to receive the frames buffered at the AP if the received TIM indicates that the AP has buffered frames for them, or they can sleep again otherwise. The doze period is defined as the time from the start of the doze state

Manuscript received August 16, 2013; revised January 8, 2014 and March 6, 2014; accepted April 17, 2014. Date of publication April 23, 2014; date of current version January 13, 2015. This work was supported in part by the Natural Science Foundation of China under Grant 61379124, Grant 61070190, and Grant 61001126 and in part by the Ph.D. Programs Foundation of the Ministry of Education of China under Grant 20123317110002. The review of this paper was coordinated by Prof. F. R. Yu.

Y.-H. Zhu and K. Chi are with the School of Computer Science and Technology, Zhejiang University of Technology, Hangzhou 310023, China (e-mail: yhzhu@zjut.edu.cn; kkchi@zjut.edu.cn).

S. Luan is with the School of Computer Science and Technology, Zhejiang University of Technology, Hangzhou 310023, China, and also with the College of Information Engineering, Hangzhou Dianzi University, Hangzhou 310018, China (e-mail: luanshenji@163.com).

V. C. M. Leung is with the Department of Electrical and Computer Engineering, The University of British Columbia, Vancouver, BC V6T 1Z4, Canada (e-mail: vleung@ece.ubc.ca).

Color versions of one or more of the figures in this paper are available online at http://ieeexplore.ieee.org.

Digital Object Identifier 10.1109/TVT.2014.2319456

at an STA to the time that it wakes up to receive the TIM. Clearly, a longer doze period consumes less energy, but it causes longer packet delays in addition to expending more memory at the AP for buffering incoming frames. Generally, memory overflow at the AP causes some buffered frames to be discarded, which evokes the source nodes to resend the corresponding lost packets, thus increasing packet delay and causing the extra energy consumed in receiving the resent packets. Therefore, efficient power management should be able to address the tradeoff among the power consumption at the STAs, the packet delay, and the memory usage at the AP. In fact, the tradeoff between the power consumption at the STAs and the memory usage at the AP has been addressed by the timer-based power management (TPM) presented in our previous work [5], which extends the BPM defined in the IEEE 802.11 standard by introducing two timers: the idle timer and the doze timer. By adjusting the values of the two timers, i.e., the parameters T_I and T_D, TPM is able to balance the power consumption and the memory usage for the AP to buffer the frames destined for the sleeping STAs.

Nowadays, Wi-Fi-enabled portable smart phones that are equipped with some sensors have become increasingly popular. For example, the Samsung Galaxy smart phone includes more than ten kinds of sensors, such as temperature and humidity sensors, an accelerometer, and a gyroscope. Many applications have been developed to use the sensors embedded in the smart phones. Consider an application that uses the embedded temperature sensor to detect a fire. In this case, the radio transceiver in the smart phone can sleep for a long time, except when abnormal temperature is detected, and the radio transceiver needs to immediately wake up if the detected high temperature indicates a possible fire. Consider another application in which a Wi-Fi device with sensors is used to monitor the movement of a patient; in this case, the radio transceiver is required to immediately wake up to transmit a message asking for help when the embedded sensor captures the event that the patient has fallen down and no longer move. In fact, there are many similar applications that share the common feature that the downlink traffic is delay tolerant, whereas the uplink traffic is delay intolerant.

Furthermore, in the applications in Internet-of-Things (IoT), different sensors with low-power radios are deployed to collect data from the environment. The IEEE 802.15.4 standard [6] is adopted in the MAC and PHY layers of wireless sensor networks (WSNs). This standard targets the compatible interconnection for data communication devices (e.g., sensors or actuators) using low-data-rate, low-power, and low-complexity short-range radio frequency transmission in a wireless personal area network [6], which makes it possible for a sensor node to work several months or years without replacing its battery. In IoT, it is required to attach IP addresses to everyday objects, allowing people to remotely communicate with and control networked devices. Naturally, Wi-Fi-enabled sensors are excellent candidates to be used in IoT since they have the advantages of easy integration with existing infrastructure, built-in IP-network compatibility, and familiar protocols and management tools [7]. The applications of Wi-Fi-enabled sensors and those of Wi-Fi coexisting with 802.15.4-based sensors can be found in [8]–[10]. Typically, Wi-Fi-enabled sensors incorporate at least two wireless interfaces: One is the Wi-Fi interface, which supports the IEEE 802.11 standard, and the other is the low-power interface, which supports the IEEE 802.15.4 standard, so that data packets can be transmitted with a high data rate via the Wi-Fi interface, while the communications between low-power devices are conducted via the low-power interface. Obviously, the Wi-Fi interface expends much more energy than the low-power interface. Therefore, it is significant to design a power management scheme to save the energy expended by the radio transceiver in the Wi-Fi interface of the Wi-Fi-enabled sensor used in event-triggered sensing applications possessing the delay-intolerant uplink traffic (DIUT) property.

Unfortunately, TPM [5] does not well support DIUT applications due to the shortcoming that, when an STA is dozing (i.e., its radio transceiver is turned off), outgoing frames are kept in a buffer in the MAC layer and not transmitted until the doze period of the STA expires. Obviously, a larger doze period may cause a critical event to be missed, although it makes the STA sleep longer and achieves more energy saving, whereas a smaller doze period wastes energy as the STA has to frequently wake up. Considering that sensors are usually used to capture random events, such as the fire detection or detecting the fall of a patient as previously mentioned, which are hard to predict, it is not easy to set a suitable length of doze period for the STA so that the events are captured and reported by the STA in a timely manner while the STA's energy is significantly saved. Therefore, the best choice is to let the transceiver of the STA wake up as soon as an event is captured. This motivates us to improve TPM and propose the enhanced TPM (E-TPM), in which the STA terminates sleeping whenever an outgoing frame is generated so that DIUT is transmitted without extra delay. To the best of our knowledge, none of the power management schemes presented for the 802.11 infrastructure WLAN in the literature have considered supporting the applications with DIUT.

The main contributions of this paper are as follows.

1) E-TPM is developed, which is able to considerably reduce packet delay such that it is applicable to applications with DIUT.
2) A stochastic model is presented to analyze the performance of the proposed E-TPM.
3) The statistics relative to the STA's operation modes are derived, including the probabilities of the STA being in the transmitting/receiving, idle, and doze modes, power consumption of the STA, number of the frames buffered at the AP during the STA's doze mode, and the average delay per frame.
4) The optimization problem used to find the values of the two timers embedded in the E-TPM is presented so that power consumption is minimized while packet delay is controlled within a preset time period given limited memory space available in the AP.

The remainder of this paper is organized as follows: Related works are surveyed in Section II, and the E-TPM applicable to IEEE 802.11 infrastructure WLANs is presented in Section III. Based on stochastic analysis, we model the power management algorithm and derive statistics in Section IV. Analysis of

numerical results and optimization of the idle timer and doze duration are conducted in Section V. Conclusions are given in Section VI.

II. Related Works

Hitherto, power saving has been intensively studied. In [3], a quorum-based sleep/wake-up mechanism is applied to conserve energy in single-hop mobile *ad hoc* networks (MANETs). The design of power-saving protocols for MANETs that allow STAs to switch to a low-power doze mode is considered in [11]. Based on the IEEE 802.11 point coordination function, the pointer-controlled slot-allocation and resynchronization protocol is proposed to reduce energy consumption by removing the need for power-saving STAs to remain awake and listen to the channel [12]. A scheduled power-saving mode (PSM) protocol is proposed in [13], which schedules APs to deliver pending data at designated time slices and adjusts the power state of mobile STAs adaptively. Synchronous wake-up patterns of networked nodes with two different service disciplines, i.e., exhaustive and gated, are modeled by means of a vacation model from queuing theory [14]. A power-saving mechanism that dynamically adjusts the sleeping strategy of nodes is given in [15]. A system called Percy aiming to maximize energy saving is presented in [16], in which the trace collected from ten iPhone users at William Marsh Rice University, Houston, TX, USA, is used. M/G/1/K queues with multiple vacations and an attention span are used to model timeout-driven power management policies [17].

As previously mentioned, an STA in doze mode expends much less power than when it is in the transmitting/receiving or idle mode. Thus, increasing the duration of the sleep state is the main energy-saving strategy in the basic power management scheme given in the IEEE 802.11 standard. In addition, the IEEE 802.11 standard specifies a constraint on an AP to buffer the downlink traffic for at least one listen interval (LI) whose length is negotiated by the power-saving STA when it associates with the AP [1]. Thus, managing active and doze periods at an STA and the allocation of frame buffers at the associated AP are significant issues that need to be addressed for power management to be effective and efficient. Idle-period predictions are exploited for the STAs to switch from active to sleep states [18]. The intelligent PSM that determines dynamic activation times based on the state of the mobile user is presented in [19] to increase energy conservation through the decision-making algorithm. A system model for infrastructure Wi-Fi networks aiming to reduce consumed power is proposed in [20], which introduces a channel-allocation scheme under the energy-conserving criterion. A scheduling policy is presented in [21] to assign APs into different subclusters so that APs properly control Wi-Fi stations to switch states between sleep and active so as to avoid packet receiving time overlapping and make energy expended efficiently. It is pointed out in [22] that more energy may be saved either by buffering packets or by allowing the STA to wake up less frequently and retrieve all the buffered packets during a single beacon interval (BI) if the traffic condition is taken into account. A buffer management scheme for the nodes in an infrastructure WLAN to effectively and efficiently save power is provided in [23]. Wang *et al.* [24] stated that reducing power consumption while maintaining the response time constraint has been an important goal in server system design.

The TPM proposed in our previous work [5] exhibits a shortcoming. That is, the packets generated by the STA during the doze period are kept in its local buffer, which introduces extra packet delay and causes the TPM to not be used in DIUT applications. This shortcoming is remedied by the proposed E-TPM, in which the STA operating in doze mode switches to the active state and transmits right away when an outgoing frame is generated by the STA rather than puts the outgoing frame in its buffer, thus reducing packet delay. The proposed E-TPM fills the void in power management for the DIUT applications in the infrastructure WLAN.

III. Enhanced Timer-Based Power Management

First, we describe the similarities and differences between TPM [5] and E-TPM. Both TPM and E-TPM have two timers, which are called the idle timer and the doze timer. The former is used to determine the instant when the STA enters doze mode, i.e., the STA begins to sleep when the idle timer expires; the latter is used to determine the instant when the STA wakes up, i.e., the STA switches to active state from doze state when the doze timer expires. The values of the idle timer and the doze timer are set to parameters T_I and T_D, respectively.

It is required in [2] that parameter T_D is set to the LI, which is equal to some multiples of the BI, and the LI is contained in the association request frame sent to the AP from the STA before the STA joins the infrastructure WLAN. Of course, the association request may be rejected by the AP if the AP does not have enough memory to buffer the incoming frames destined to the sleeping STA within the doze period of the LI (i.e., T_D). In a word, the value of T_D cannot be determined until the STA has negotiated with the AP, and the association request is granted. The value of T_I, however, can be settled by the STA without permission from the AP.

The main difference between the TPM and the E-TPM is shown in Fig. 1. The timelines in TPM are shown in Fig. 1(a), in which the vertical lines crossing the horizontal timelines represent the beacons, with interval BI between them, each including a TIM being announced by the AP. "TIM: 1" represents the presence of frames in the AP buffer, whereas "TIM: 0" means no frame is buffered. A triangle stands for the waking up of the STA. It can be seen in the figure that, at time t_1, the AP announces "TIM:1," which leads the STA to send a PS-Poll frame to the AP to retrieve a buffered frame, and then, a buffered data frame is sent from the AP to the STA (more PS-Poll frames to the AP are needed if there are more frames buffered [1]). At time t_2, the STA retrieves all the buffered frames and enters the idle state until time t_3. That is, the STA stays idle for the period of T_{I0}, referred to as the mandatory idle time (MIT), which lasts from the instant when the STA becomes idle to the instant when the next beacon ends. TPM differs from BPM in that, under BPM, the STA enters the doze mode after the MIT has expired (i.e., the STA begins sleeping at time t_3); however, under TPM, the STA is forced to stay idle for a longer period, i.e., T_{I1} in the figure, which is referred to as prolonged idle time (PIT) and is set to be some multiples of the BI. In this figure,

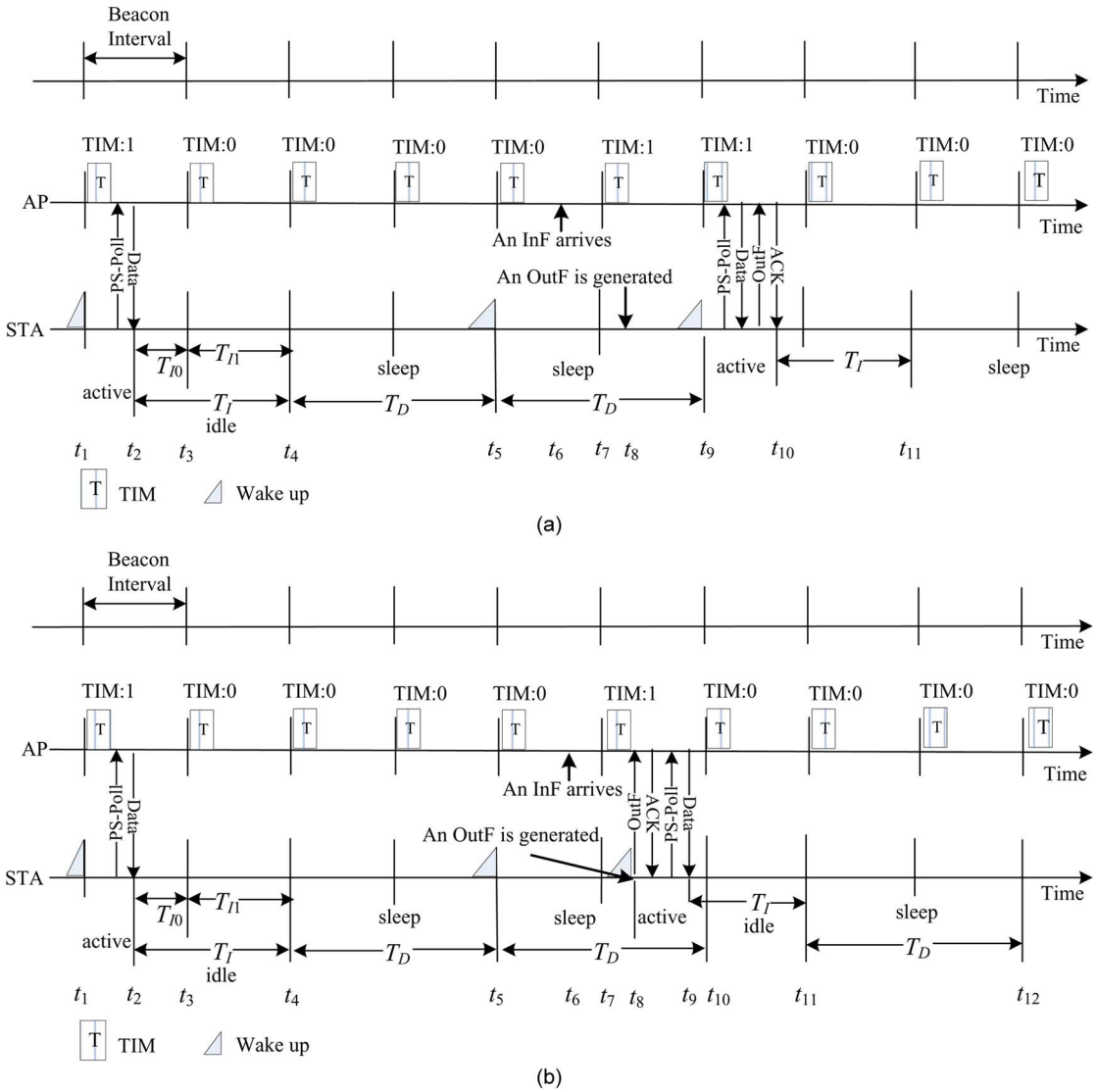

Fig. 1. Timelines of the (a) TPM and the (b) proposed E-TPM.

we set PIT to BI and the doze period $T_D = 2$BI. With TPM, the STA begins to sleep for the period of T_D (i.e., 2BI) at time t_4. At time t_5, it wakes up to receive the beacon and sleeps for the period of T_D again as "TIM:0" indicates that no frame is buffered at the AP. An incoming frame (InF) arrives at time t_6, which causes the AP to announce "TIM:1" in the beacon at time t_7; however, the STA does not receive the beacon since it stays in doze mode that time. At time t_8, an outgoing frame (OutF) is generated; however, the STA puts the OutF in the buffer and continues to sleep. The STA wakes up at time t_9 on schedule to receive the TIM, and then, it stays awake to receive the InF and transmits the OutF. At time t_{10}, it becomes idle again. The STA enters doze mode at time t_{11} after $T_I = \text{MIT} + \text{PIT}$ has elapsed, and so forth.

The shortcoming of the TPM can be clearly observed in Fig. 1(a) that, at time t_8, an OutF is generated by the STA, but this OutF is buffered and transmitted after time t_9, which delays the OutF. As a result, much more delay is introduced if more OutFs are generated during the doze period, which may not be tolerable for some DIUT applications.

The given shortcoming of TPM is overcome by E-TPM, in which the STA terminates sleeping whenever an OutF is generated so that the delay is reduced. The timelines of E-TPM are shown in Fig. 1(b), where the STA wakes up at time t_8 when an OutF is generated so that the OutF is transmitted right away to the AP, and meanwhile, the AP piggybacks the presence of the buffered frame (i.e., the InF) to the STA in the ACK frame so that the STA can send a PS-Poll frame to the AP to retrieve the buffered InF, thus reducing the InF delay as well. In a word, the key difference between E-TPM and TPM lies in that the STA with E-TPM immediately wakes up whenever an OutF is generated, whereas the STA with TPM definitely sleeps for a fixed period of T_D.

Next, we describe E-TPM in detail. E-TPM consists of two parts: One runs in the STA, called E-TPM-STA, and the other runs in the AP, called E-TPM-AP. The flowchart of E-TPM-STA is shown in Fig. 2, where N_FBAS represents the total number of frames buffered by the AP and the STA. The flowchart of E-TPM-AP is given in Fig. 3 [5], where *SMem* is the size of the memory (in frames) allocated to buffer the frames

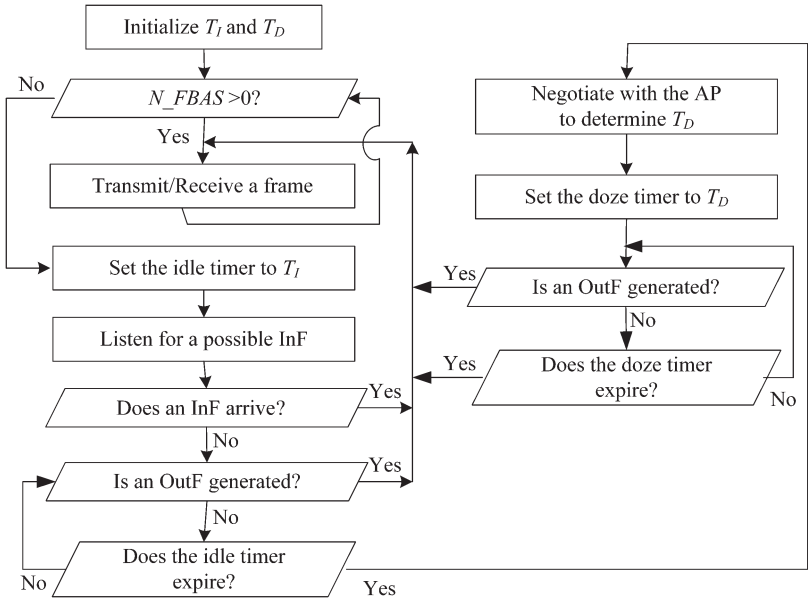

Fig. 2. Power management algorithm running at the STA.

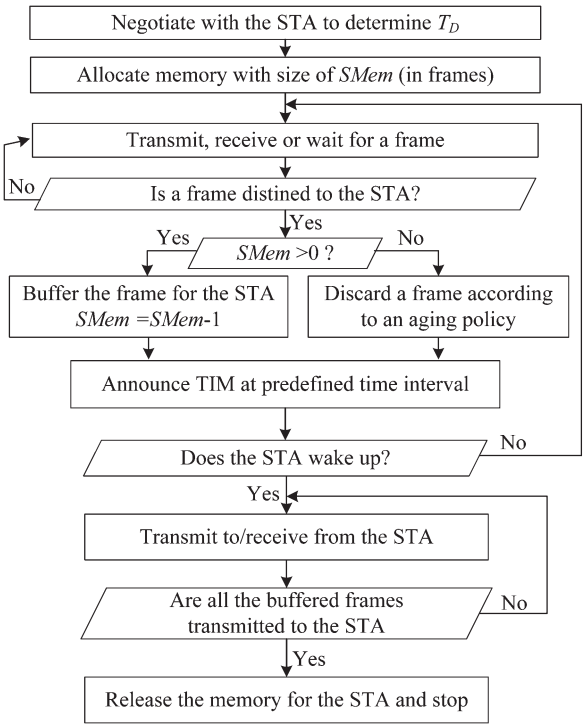

Fig. 3. Power management algorithm running at the AP [5].

destined to the STA at the AP when the STA operates in doze mode.

Under E-TPM-STA, the STA enters the idle state and starts the idle timer with the duration of T_I when it finishes transmitting all the OutFs in its buffer and receiving all the InFs from the AP. The STA cancels the idle timer and starts to transmit or receive whenever an InF arrives or an OutF is generated. If no frame arrives before the idle timer times out, the STA initiates dozing with the doze timer set to the time duration of T_D. The STA terminates its doze mode when an OutF is generated by itself. Moreover, the STA wakes up to listen to the next TIM frame when the doze timer times out (i.e., the time spent in doze mode has reached T_D). If there is any buffered frame at the AP (as indicated by the TIM) at the end of the doze period, the STA begins to receive the InFs buffered at the AP; otherwise, it starts another doze period with the same time duration of T_D.

E-TPM-AP is invoked when the AP receives an STA's request to doze. The AP sets the doze duration to T_D by negotiating with the STA and allocates enough memory for buffering *SMem* frames destined to the STA. This memory will be released when the STA has received all the InFs buffered at the AP after it finishes dozing.

It can be seen in Figs. 2 and 3 that parameters T_I and T_D are heavily related to whether the E-TPM is efficiently and effectively applied or not. Hence, how to set a suitable pair of parameters T_I and T_D as to reduce delay and save energy with a given memory size at the AP becomes a critical issue for E-TPM, which will be addressed by the optimization problem given in (30) in Section V.

IV. Statistics of Enhanced Timer-Based Power Management

We only consider the energy consumption of an STA's wireless interface, which, as previously mentioned, depends on the STA's operating mode: transmitting, receiving, idle, or doze. For tractability of the analysis, we combine transmitting and receiving modes into a single state called the active state when the STA operates in either one of these two modes [5], [23]. Moreover, the active state is further divided into the following substates: $A_0, A_1, \ldots$, where A_n $(n = 0, 1, \ldots)$ represents the state of the STA when it is busy in transmitting/receiving a frame while there are n other frames waiting for transmission/reception by the STA. Similarly, the doze state is divided into the following substates: $D_0, D_1, \ldots$, where $D_n (n = 0, 1, \ldots)$ represents the state of the STA when it is in doze mode, and n frames are buffered at the AP. The transitions among the given states are shown in Fig. 4, in which the circles represent the

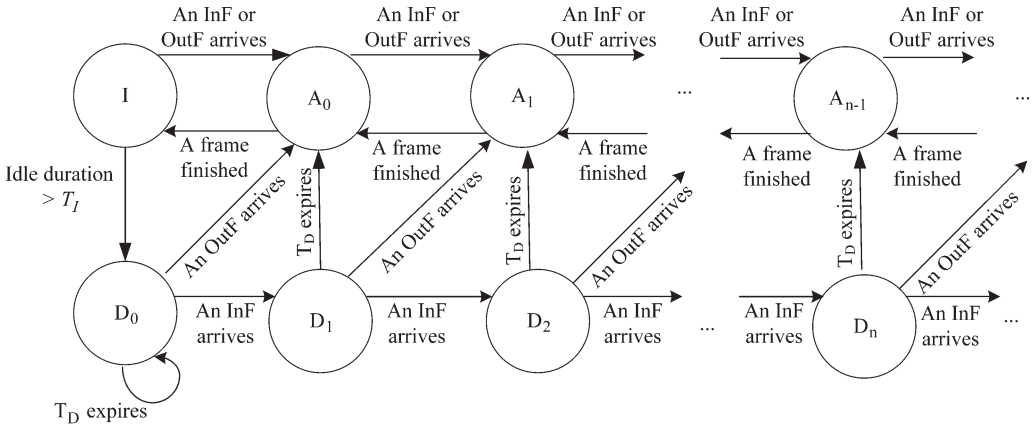

Fig. 4. State-transition diagram.

states of the STA. In particular, the circle labeled with letter "I" represents the idle state.

A. Assumptions

Assume that there are N STAs in the WLAN. In addition, for the kth STA $(k = 1, 2, \ldots, N)$, assume [5] the following.

i) The doze period of the kth STA is a random variable, which is denoted by $\chi_D^{(k)}$, with expectation $E[\chi_D^{(k)}] = 1/\eta^{(k)}$ (i.e., $\eta^{(k)}$ is the expected number of dozing per unit of time), second moment $E[(\chi_D^{(k)})^2] \equiv \alpha^{(k)}$, probability density function (pdf) $g^{(k)}(x)$, and cumulative distribution function (cdf) $G^{(k)}(x)$. In addition, the hazard rate function [25] of $\chi_D^{(k)}$ is $\tau^{(k)}(x) \equiv g^{(k)}(x)/\overline{G}^{(k)}(x)$, where $\overline{G}^{(k)}(x) \equiv 1 - G^{(k)}(x)$. Here, the symbol "$\equiv$" means "is defined as."

ii) The time consumed by the kth STA to transmit/receive a frame, which is either the time period from the instant when the STA begins competing for accessing the channel to the instant when the frame is completely transmitted or the time period from the instant when the STA begins receiving the frame to the instant when the frame is completely received, is a random variable $\chi^{(k)}$, with $E[\chi^{(k)}] \equiv 1/\mu^{(k)}$ (i.e., $\mu^{(k)}$ is the expected number of frames transmitted/received per unit of time) and $E[(\chi^{(k)})^2] \equiv \beta^{(k)}$. The pdf, cdf, and the hazard rate function of $\chi^{(k)}$ are, respectively, denoted by $f^{(k)}(x)$, $F^{(k)}(x)$, and $\sigma^{(k)}(x) \equiv f^{(k)}(x)/\overline{F}^{(k)}(x)$, where $\overline{F}^{(k)}(x) \equiv 1 - F^{(k)}(x)$.

iii) New InFs to the kth STA form a Poisson process with rate $\lambda_1^{(k)}$, and new OutFs from the STA form a Poisson process with rate $\lambda_2^{(k)}$ [5], [17], [23]. Equivalently, the time interval of the new InFs to the kth STA, which is denoted by $\chi_{\mathrm{InF}}^{(k)}$, and that of new OutFs from the kth STA, which is denoted by $\chi_{\mathrm{OutF}}^{(k)}$, are exponential distributions with rate parameters $\lambda_1^{(k)}$ and $\lambda_2^{(k)}$, respectively.

Assume that random variable $\chi^{(k)}$ is independent from random variables $\chi_{\mathrm{InF}}^{(k)}$ and $\chi_{\mathrm{OutF}}^{(k)}$, random variables $\chi_D^{(k)}$ and $\chi_{\mathrm{InF}}^{(k)}$ are independent, and $\chi_{\mathrm{InF}}^{(k)}$ and $\chi_{\mathrm{OutF}}^{(k)}$ are independent, where $k = 1, 2, \ldots, N$. Define $\rho^{(k)} = \lambda^{(k)}/\mu^{(k)}$, where $\lambda^{(k)} = \lambda_1^{(k)} + \lambda_2^{(k)}$. We consider only cases where $\rho^{(k)} < 1$ to prevent the buffer occupancy from growing without bound [5].

B. Model

Let Ω be the set of all possible states of the STA. For the kth STA $(k = 1, 2, \ldots, N)$, we use $\xi^{(k)}(t)$ to denote its state at time t and $X^{(k)}(t)$ be its accumulated state residence time, i.e., the amount of time that the STA has spent in the current state until time t. For $u \in \Omega$, $u \neq I$, events $\xi^{(k)}(t) = u$ and $X^{(k)}(t) = x$ at time t has a joint pdf $p_u^{(k)}(t, x)$, which satisfies

$$p_u^{(k)}(t,x)dx = \Pr\left\{\xi^{(k)}(t) = u, x < X^{(k)}(t) \leq x + dx\right\}. \quad (1)$$

Thus

$$P_{A_n}^{(k)}(t) \equiv \Pr\left\{\xi^{(k)}(t) = A_n\right\} = \int_0^\infty p_{A_n}^{(k)}(t,x)dx \quad (2)$$

$$P_{D_n}^{(k)}(t) \equiv \Pr\left\{\xi^{(k)}(t) = D_n\right\} = \int_0^\infty p_{D_n}^{(k)}(t,x)dx. \quad (3)$$

Let $P_{A_n}^{(k)} \equiv \lim_{t\to\infty} P_{A_n}^{(k)}(t)$ and $P_{D_n}^{(k)} \equiv \lim_{t\to\infty} P_{D_n}^{(k)}(t)$, $n = 0, 1, \ldots$. In addition, let $P_I^{(k)}(t) \equiv \Pr\{\xi^{(k)}(t) = I\}$ and $P_I^{(k)} \equiv \lim_{t\to\infty} P_I^{(k)}(t)$. Hence, the probabilities of the kth STA being in active and doze states are $P_A^{(k)} \equiv \sum_{n=0}^\infty P_{A_n}^{(k)}$ and $P_D^{(k)} \equiv \sum_{n=0}^\infty P_{D_n}^{(k)}$, respectively. Moreover, the generating functions of $\chi_D^{(k)}$ and $\chi^{(k)}$ are $K^{(k)}(z) \equiv \sum_{n=0}^\infty P_{A_n}^{(k)} z^n$ and $Q^{(k)}(z) \equiv \sum_{n=0}^\infty P_{D_n}^{(k)} z^n$, respectively, where $|z| < 1$. Furthermore, we introduce two *z-transforms* for the kth STA as follows:

$$K^{(k)}(t,x,z) \equiv \sum_{n=0}^\infty p_{A_n}^{(k)}(t,x)z^n, \quad (|z| < 1) \quad (4)$$

$$Q^{(k)}(t,x,z) \equiv \sum_{n=0}^\infty p_{D_n}^{(k)}(t,x)z^n, \quad (|z| < 1). \quad (5)$$

Let $\chi_I^{(k)}$ be the duration from the instant when the kth STA enters the idle state to the instant when the next InF or OutF

arrives. In addition, we use $T_I^{(k)}$ and $T_D^{(k)}$ to denote the values of the idle timer and the doze timer of the kth STA, respectively. Thus, we have the following equation [5], where $o(\Delta t)$ is an infinitesimal satisfying $\lim_{\Delta t\to 0} o(\Delta t)/\Delta t = 0$:

$$\Pr\left\{\chi_I^{(k)} + \Delta t \geq T_I^{(k)} \,|\, \chi_I^{(k)} < T_I^{(k)}\right\} = \frac{\lambda^{(k)} e^{-\lambda^{(k)} T_I^{(k)}} \Delta t}{1 - e^{-\lambda^{(k)} T_I^{(k)}}} + o(\Delta t). \quad (6)$$

Considering the state transitions during time interval Δt in Fig. 4, making use of (6), and then letting Δt approach 0, we have the following equations for the kth STA (the derivations are similar to those found in [5, App. I]):

$$\left[\frac{\partial}{\partial t} + \frac{\partial}{\partial x} + \lambda^{(k)} + \sigma^{(k)}(x)\right] p_{A_0}^{(k)}(t,x) = 0 \quad (7)$$

$$\left[\frac{\partial}{\partial t} + \frac{\partial}{\partial x} + \lambda^{(k)} + \sigma^{(k)}(x)\right] p_{A_n}^{(k)}(t,x) = \lambda^{(k)} p_{A_{n-1}}^{(k)}(t,x) \quad n = 1,2,\ldots \quad (8)$$

$$\left[\frac{\partial}{\partial t} + \frac{\partial}{\partial x} + \lambda^{(k)} + \tau^{(k)}(x)\right] p_{D_0}^{(k)}(t,x) = 0 \quad (9)$$

$$\left[\frac{\partial}{\partial t} + \frac{\partial}{\partial x} + \lambda^{(k)} + \tau^{(k)}(x)\right] p_{D_n}^{(k)}(t,x) = \lambda_1^{(k)} p_{D_{n-1}}^{(k)}(t,x) \quad n = 1,2,\ldots \quad (10)$$

$$p_{A_0}^{(k)}(t,0) = \int_0^\infty p_{A_1}^{(k)}(t,x)\sigma^{(k)}(x)dx + \lambda^{(k)} P_I^{(k)}(t) + \lambda_2^{(k)} \int_0^\infty p_{D_0}^{(k)}(t,x)dx + \int_0^\infty p_{D_1}^{(k)}(t,x)\tau^{(k)}(x)dx \quad (11)$$

$$p_{A_n}^{(k)}(t,0) = \int_0^\infty p_{A_{n+1}}^{(k)}(t,x)\sigma^{(k)}(x)dx + \lambda_2^{(k)} \int_0^\infty p_{D_n}^{(k)}(t,x)dx + \int_0^\infty p_{D_{n+1}}^{(k)}(t,x)\tau^{(k)}(x)dx \quad (12)$$

$$p_{D_0}^{(k)}(t,0) = P_I^{(k)}(t)\frac{\lambda^{(k)} e^{-\lambda^{(k)} T_I^{(k)}}}{1 - e^{-\lambda^{(k)} T_I^{(k)}}} + \int_0^\infty p_{D_0}^{(k)}(t,x)\tau^{(k)}(x)dx \quad (13)$$

$$p_{D_n}^{(k)}(t,0) = 0, \qquad n = 1,2,\ldots \quad (14)$$

$$\left[\frac{d}{dt} + \frac{\lambda^{(k)}}{1 - e^{-\lambda^{(k)} T_I^{(k)}}}\right] P_I^{(k)}(t) = \int_0^\infty p_{A_0}^{(k)}(t,x)\sigma^{(k)}(x)dx. \quad (15)$$

We assume that the STA stays in the idle state at time $t = 0$. That is, the initial conditions are

$$P_I^{(k)}(0) = 1; \qquad p_{A_i}^{(k)}(0,x) = 0, \quad p_{D_i}^{(k)}(0,x) = 0 \quad i = 0,1,\ldots. \quad (16)$$

C. State Residency Probabilities and Statistics of E-TPM

Solving the set of (6)–(16), we obtain the following state residency probabilities for the kth STA (see Appendix A for the detailed derivation):

$$P_A^{(k)} = \rho^{(k)} \quad (17)$$

$$P_I^{(k)} = \lambda_2^{(k)}\left[1 - g^*\left(\lambda^{(k)}\right)\right]\left(1 - e^{-\lambda^{(k)} T_I^{(k)}}\right) \times \left(1 - \rho^{(k)}\right) \Big/ \left\{\lambda_2^{(k)}\left[1 - g^*\left(\lambda^{(k)}\right)\right]\left(1 - e^{-\lambda^{(k)} T_I^{(k)}}\right) + \lambda^{(k)}\left[1 - g^*\left(\lambda_2^{(k)}\right)\right] e^{-\lambda^{(k)} T_I^{(k)}}\right\} \quad (18)$$

$$P_D^{(k)} = \lambda^{(k)} e^{-\lambda^{(k)} T_I^{(k)}}\left[1 - g^*\left(\lambda_2^{(k)}\right)\right] \times \left(1 - \rho^{(k)}\right) \Big/ \left\{\lambda_2^{(k)}\left[1 - g^*(\lambda^{(k)})\right]\left(1 - e^{-\lambda^{(k)} T_I^{(k)}}\right) + \lambda^{(k)}\left[1 - g^*\left(\lambda_2^{(k)}\right)\right] e^{-\lambda^{(k)} T_I^{(k)}}\right\} \quad (19)$$

where $P_A^{(k)}$, $P_I^{(k)}$, and $P_D^{(k)}$ are the probabilities of the kth STA staying at the active, idle, and doze states, respectively.

It can be clearly seen from (17) that the probability of the kth STA staying in the active state, i.e., $P_A^{(k)}$, depends only on $\lambda^{(k)}$ and $\mu^{(k)}$ due to $\rho^{(k)} = \lambda^{(k)}/\mu^{(k)}$ rather than on $T_I^{(k)}$ and $T_D^{(k)}$. In other words, the values of the idle timer and the doze timer do not affect the probability $P_A^{(k)}$. Moreover, from (18) and (19), we observe that $P_D^{(k)}$ and $P_I^{(k)}$ can be determined only when $g^*(\lambda^{(k)})$ and $g^*(\lambda_2^{(k)})$ are found. Obviously, the pdf of $\chi_{\mathrm{OutF}}^{(k)}$ is $\lambda_2^{(k)} e^{-\lambda_2^{(k)} x}$ [25]. As previously mentioned, E-TPM differs from TPM as presented in [5] in that the STA wakes up to transmit right away if an OutF is generated. In other words, when the STA operates in doze mode, if an OutF arrives in the time period of $T_D^{(k)}$, which has the probability of $1 - e^{-\lambda_2^{(k)} T_D^{(k)}}$, the STA sleeps for the period of $\chi_{\mathrm{OutF}}^{(k)}$; otherwise, it sleeps for a fixed period of $T_D^{(k)}$. Considering that only when no OutF is generated during the STA's doze period, which has the probability of $e^{-\lambda_2^{(k)} T_D^{(k)}}$, does the STA sleep for a fixed period of $T_D^{(k)}$, whose pdf is the Dirac delta function $\delta(x - T_D^{(k)})$ [5]. Hence, we obtain the pdf of $\chi_D^{(k)}$ as follows:

$$g^{(k)}(x) = \lambda_2^{(k)} e^{-\lambda_2^{(k)} x} u(x) + e^{-\lambda_2^{(k)} T_D^{(k)}} \delta\left(x - T_D^{(k)}\right) \quad (20)$$

in which we define $u(x) = \begin{cases} 1, & x \leqslant T_D^{(k)} \\ 0, & x > T_D^{(k)} \end{cases}$. Thus, from the Laplace–Stieltjes transform (LST) of $g^{(k)}(x)$, we obtain (see Appendix A for the definition of LST)

$$g^{(k)*}\left(\lambda^{(k)}\right) = \frac{\lambda_2^{(k)} + \lambda^{(k)} e^{-\left(\lambda^{(k)} + \lambda_2^{(k)}\right) T_D^{(k)}}}{\lambda^{(k)} + \lambda_2^{(k)}}$$

$$g^{(k)*}\left(\lambda_2^{(k)}\right) = \frac{1}{2}\left(1 + e^{-2\lambda_2^{(k)} T_D^{(k)}}\right) \quad (21)$$

$$E\left[\chi_D^{(k)}\right] = \frac{1}{\eta^{(k)}} = \int_0^\infty x g^{(k)}(x)dx = \frac{1}{\lambda_2^{(k)}}\left(1 - e^{-\lambda_2^{(k)} T_D^{(k)}}\right). \quad (22)$$

Substituting (21) into (18) yields

$$P_I^{(k)} = 2\lambda_2^{(k)}\left(1-e^{-\left(\lambda^{(k)}+\lambda_2^{(k)}\right)T_D^{(k)}}\right) \times \left(1-e^{-\lambda^{(k)}T_I^{(k)}}\right)\left(1-\rho^{(k)}\right) \Big/ \left\{2\lambda_2^{(k)}\left(1-e^{-\left(\lambda^{(k)}+\lambda_2^{(k)}\right)T_D^{(k)}}\right)\left(1-e^{-\lambda^{(k)}T_I^{(k)}}\right) + \left(\lambda^{(k)}+\lambda_2^{(k)}\right)\left(1-e^{-2\lambda_2^{(k)}T_D^{(k)}}\right)e^{-\lambda^{(k)}T_I^{(k)}}\right\}. \quad (23)$$

We denote the average power consumption of the STA by $E_{\text{avg}}^{(k)}$, the average number of frames waiting for transmission at the STA and the AP when the STA is active by $N_{\text{Wait-ETPM}}^{(k)}$, the average delay per frame when the STA is active by $T_{\text{Delay-ETPM}}^{(k)}$, and the average value of N_FBAS when the STA is dozing by $N_{\text{Buffer-ETPM}}^{(k)}$. Then, we obtain the properties of the model for the kth STA, which are given in (24)–(28), shown below (see Appendix B for the proof)

$$P_A^{(k)} = \rho^{(k)}, \quad P_D^{(k)} = 1-\rho^{(k)}-P_I^{(k)} \quad (24)$$

$$E_{\text{avg}}^{(k)} \equiv P_A^{(k)}E_A^{(k)} + P_D^{(k)}E_D^{(k)} + P_I^{(k)}E_I^{(k)} = \rho^{(k)}E_A^{(k)} + \left(1-\rho^{(k)}\right)E_D^{(k)} + \left(E_I^{(k)} - E_D^{(k)}\right)P_I^{(k)} \quad (25)$$

where $E_I^{(k)}$, $E_D^{(k)}$, and $E_A^{(k)}$ are the STA's power consumption in the idle, doze, and active states, respectively

$$N_{\text{Wait-ETPM}}^{(k)} = \frac{(\lambda^{(k)})^2\beta^{(k)}}{2(1-\rho^{(k)})} + \rho^{(k)}\lambda_1^{(k)}\left(\lambda^{(k)}+\lambda_2^{(k)}\right)e^{-\lambda^{(k)}T_I^{(k)}} \times \left[\left(1-e^{-2\lambda_2^{(k)}T_D^{(k)}}\right) - 2\lambda_2^{(k)}T_D^{(k)}e^{-2\lambda_2^{(k)}T_D^{(k)}}\right] \Big/ \left\{2\lambda_2^{(k)}\left[2\lambda_2^{(k)}\left(1-e^{-\lambda^{(k)}T_I^{(k)}}\right)\left(1-e^{-\left(\lambda^{(k)}+\lambda_2^{(k)}\right)T_D^{(k)}}\right) + \left(\lambda^{(k)}+\lambda_2^{(k)}\right)e^{-\lambda^{(k)}T_I^{(k)}}\left(1-e^{-2\lambda_2^{(k)}T_D^{(k)}}\right)\right]\right\} \quad (26)$$

$$T_{\text{Delay-ETPM}}^{(k)} = \left(\left\lceil N_{\text{Wait-ETPM}}^{(k)}\right\rceil + 1\right) \Big/ \left(2\mu^{(k)}\right) \quad (27)$$

where $\lceil\ \rceil$ is the ceiling function.

$$N_{\text{Bufferred-ETPM}}^{(k)} = \left(1-\rho^{(k)}\right)\lambda_1^{(k)}\left(\lambda^{(k)}+\lambda_2^{(k)}\right)e^{-\lambda^{(k)}T_I^{(k)}} \times \left[\left(1-e^{-2\lambda_2^{(k)}T_D^{(k)}}\right) - 2\lambda_2^{(k)}T_D^{(k)}e^{-2\lambda_2^{(k)}T_D^{(k)}}\right] \Big/ \left\{2\lambda_2^{(k)}\left[2\lambda_2^{(k)}\left(1-e^{-\lambda^{(k)}T_I^{(k)}}\right)\left(1-e^{-\left(\lambda^{(k)}+\lambda_2^{(k)}\right)T_D^{(k)}}\right) + \left(\lambda^{(k)}+\lambda_2^{(k)}\right)e^{-\lambda^{(k)}T_I^{(k)}}\left(1-e^{-2\lambda_2^{(k)}T_D^{(k)}}\right)\right]\right\}. \quad (28)$$

Noting that both the active and the doze states contribute packet delay and that no delay is introduced in the idle state, we obtain the average delay (i.e., the expected delay) as follows using (22) and (24):

$$T_{\text{Delay}}^{(k)} \equiv P_A^{(k)}T_{\text{Delay-ETPM}}^{(k)} + P_D^{(k)}E\left[\chi_D^{(k)}\right] + P_I^{(k)} \times 0 = \rho^{(k)}T_{\text{Delay-ETPM}}^{(k)} + P_D^{(k)}\frac{1-e^{-\lambda_2^{(k)}T_D^{(k)}}}{\lambda_2^{(k)}}. \quad (29)$$

We observe that E-TPM reduce to TPM if no outF is generated, which is equivalent to $\lambda_2^{(k)} = 0$, when the STA operates in doze mode. That is, the statistics previosuly derived reduce to those derived in [5] when we let $\lambda_2^{(k)} \to 0$. In fact, it is easy to show by L'Hôpital's rule that (23)–(28) in this paper reduce to [5, Eqs. (18)–(22)] when $\lambda_2^{(k)} \to 0$, which validates the statistics derived in this paper. Due to space limitations and the similar derivation processes, we only present the limit of (23), shown at the bottom of the page, which is the same as [5, Eq. (18)].

$$\lim_{\lambda_2^{(k)}\to 0} P_I^{(k)} = 2\lambda_2^{(k)}\left(1-e^{-\left(\lambda^{(k)}+\lambda_2^{(k)}\right)T_D^{(k)}}\right)\left(1-e^{-\lambda^{(k)}T_I^{(k)}}\right)\left(1-\rho^{(k)}\right) \Big/ \left\{2\lambda_2^{(k)}\left(1-e^{-\left(\lambda^{(k)}+\lambda_2^{(k)}\right)T_D^{(k)}}\right)\left(1-e^{-\lambda^{(k)}T_I^{(k)}}\right) + \left(\lambda^{(k)}+\lambda_2^{(k)}\right)\left(1-e^{-2\lambda_2^{(k)}T_D^{(k)}}\right)e^{-\lambda^{(k)}T_I^{(k)}}\right\}$$

$$= \left(1-\rho^{(k)}\right)\left[1 + \lim_{\lambda_2^{(k)}\to 0}\frac{\left(1-e^{-2\lambda_2^{(k)}T_D^{(k)}}\right)}{2\lambda_2^{(k)}} \times \lim_{\lambda_2^{(k)}\to 0}\frac{\left(\lambda^{(k)}+\lambda_2^{(k)}\right)e^{-\lambda^{(k)}T_I^{(k)}}}{\left(1-e^{-\left(\lambda^{(k)}+\lambda_2^{(k)}\right)T_D^{(k)}}\right)\left(1-e^{-\lambda^{(k)}T_I^{(k)}}\right)}\right]^{-1}$$

$$= \left(1-\rho^{(k)}\right)\left[1 + \frac{\lambda_1^{(k)}e^{-\lambda_1^{(k)}T_I^{(k)}}T_D^{(k)}}{\left(1-e^{-\lambda_1^{(k)}T_D^{(k)}}\right)\left(1-e^{-\lambda_1^{(k)}T_I^{(k)}}\right)}\right]^{-1} = \frac{\left(1-\rho^{(k)}\right)\left(1-e^{-\lambda_1^{(k)}T_D^{(k)}}\right)\left(1-e^{-\lambda_1^{(k)}T_I^{(k)}}\right)}{\lambda_1^{(k)}T_D^{(k)}e^{-\lambda_1^{(k)}T_I^{(k)}} + \left(1-e^{-\lambda_1^{(k)}T_D^{(k)}}\right)\left(1-e^{-\lambda_1^{(k)}T_I^{(k)}}\right)}$$

V. Performance Analysis of Enhanced Timer-Based Power Management

We consider that the frame transmission duration has a Gamma distribution whose pdf is $f(x) = (\mu\gamma)^{\gamma} x^{\gamma-1} \times e^{-\mu\gamma x}/\Gamma(\gamma)$ with mean value $1/\mu$ and variance $1/(\gamma\mu^2)$ [5], [23]. The Gamma distribution is selected for its desirable property that it fits most distributions by setting appropriate parameters μ and γ. Thus, $\beta^{(k)} = (\gamma\mu + 1)/(\gamma\mu^2)$. $E_A^{(k)}$ and $E_I^{(k)}$ are much larger than $E_D^{(k)}$. We set $E_A^{(k)} = 1$ W, $E_I^{(k)} = 0.83$ W, and $E_D^{(k)} = 0.13$ W [17].

Basically, $\lambda^{(k)}$ and $\mu^{(k)}$ are determined by the traffic to/from the kth STA. Hence, we may tune $T_I^{(k)}$ and $T_D^{(k)}$ instead of $\lambda^{(k)}$ and $\mu^{(k)}$. From the theoretical and experimental outcomes, we found that E-TPM shares some properties of TPM. That is, as $T_I^{(k)}$ is decreased or $T_D^{(k)}$ is increased, E_{avg} decreases, but $N_{\text{Wait-ETPM}}^{(k)}$ and $T_{\text{Delay-ETPM}}^{(k)}$ increase, which indicate that a small $T_I^{(k)}$ or large $T_D^{(k)}$ help to save power. These properties agree with our intuition (see [5] for the explanations).

The IEEE 802.11 standard requires that, after receiving a data frame, a power-saving STA must remain awake until the next beacon is transmitted [1]. That is, $T_{I0}^{(k)}$ (see Fig. 1) is a random variable, causing $T_I^{(k)}$ to change with time. In addition, $T_{I1}^{(k)} = m\ BI$, where m is a positive integer. As a first approximation, we fix $T_I^{(k)} = E[T_{I0}^{(k)}] + T_{I1}^{(k)}$, where $E[T_{I0}^{(k)}]$ is the expectation of $T_{I0}^{(k)}$. This approximation does not significantly affect the results since $0 \le T_{I0}^{(k)} \le BI \le T_{I1}^{(k)}$. In fact, $T_{I0}^{(k)}$ can be considered as a random variable uniformly distributed in $[0, BI]$, which yields $E[T_{I0}^{(k)}] = 0.5BI$. As a result, we have $T_I^{(k)} = m\ BI + E[T_{I0}^{(k)}] = (m + 0.5)\ BI$. Noting that a small $T_I^{(k)}$ is preferred for saving power, we limit $m \le 1000$.

μ depends on the traffic (the actual frames transmitted and the access traffic load from all STAs) and the channel condition that affects the data rate. Currently, 802.11a/g-based WLANs support data rates of 6, 9, 12, 18, 24, 36, 48, and 54 Mb/s. In [26], it is shown that, at these data rates and without considering the backoff procedure and RTS/CTS control frames, the transmission times of a frame with a 1300-byte payload under 802.11a standard are 0.001936, 0.001331, 0.001011, 0.000707, 0.000554, 0.000402, 0.000326, and 0.000302 s, respectively, which are equivalent to frame transmission rates of approximately 516, 751, 989, 1414, 1805, 2488, 3068, and 3311 frames/s [23]. Therefore, as in [23], we select $\mu =$ 2000 frames per second (fps) as the nominal value.

In addition, we fix $BI = 0.1$ s [2] and $\gamma = 100$. Essentially, $T_D^{(k)}$ must be set to multiples of BI. A two-octet field is used in the management frame for the LI, i.e., the number of BIs, for a power-saving STA [2], which indicates that the maximal value of $T_D^{(k)}$ is limited to $2^{16} - 1 = 65535$. Thus, $T_D^{(k)} = j\ BI$, where $j = 1, 2, \ldots, 65535$. Additionally, we limit $j \le 3000$, i.e., the LI is bounded to 300 s or 5 min.

The proposed E-TPM focuses on reducing packet delay particularly for the uplink. Below, we compare the delay of E-TPM with that of TPM presented in [5]. We introduce the notation $\theta^{(k)} \equiv \lambda_1^{(k)}/\lambda_2^{(k)}$, which is the ratio of the downlink traffic to the uplink traffic. In event-triggered sensing applications in which Wi-Fi-enabled sensors are used to collect data from environment, downlink and uplink packets are used to carry controlling commands from the data center (or the sink) and the data sensed by the STA, respectively. Hence, the uplink traffic is usually larger than the downlink traffic, i.e., $\theta^{(k)} < 1$. Hence, we let $\theta^{(k)} = 1/10, 1/20,$ and $1/30$, which produces the delay ratio of TPM to E-TPM and power consumption ratio (PCR) of E-TPM to TPM as shown in Fig. 5, in which the superscript (k) for the kth STA is omitted and $T_I^{(k)} = 1.5BI = 0.15$ s (i.e., setting $m = 1$). In Fig. 5, we observe that, at the expense of increased energy consumption, E-TPM is able to considerably reduce delay. It is observed in Fig. 5 that the highest PCR occurs when $\rho^{(k)} = 0.006$ (see the down part in the figure), whereas the highest delay ratio of TPM to E-TPM occurs when $\rho^{(k)} = 0.022$ (see the top part of the figure).

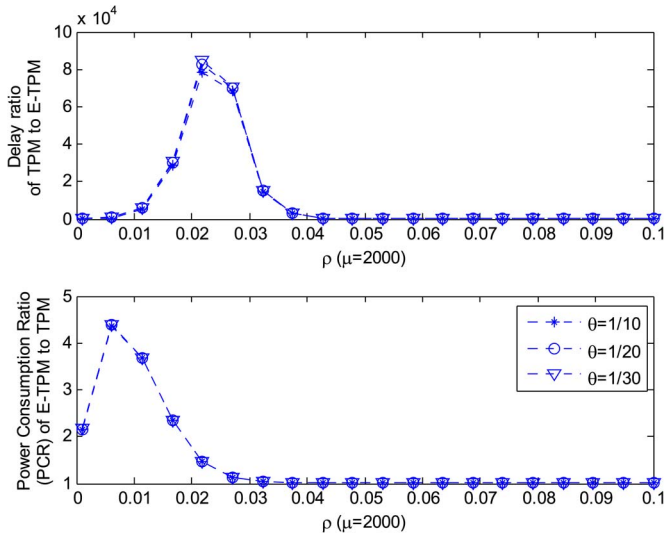

Fig. 5. Delay ratio and PCR.

To closely observe the two cases when $\rho^{(k)} = 0.006$ and $\rho^{(k)} = 0.022$, we let $\rho^{(k)}$ take two more values of 0.006 ± 0.005 close to 0.006 (i.e., $\rho^{(k)} = 0.001, 0.006, 0.011$) and two more values of 0.022 ± 0.005 close to 0.022 (i.e., $\rho^{(k)} = 0.017, 0.022,$ and 0.027), respectively, which generates Fig. 6, where the two cases with $\rho^{(k)} = 0.006$ and $\rho^{(k)} = 0.022$ are shown on the left and right sides, respectively, and delay ratio and PCR are shown in the top and down parts, respectively. It can be clearly seen on the left side of Fig. 6, even in the worst case, that PCR reaches its climax (i.e., 4.5) when $\rho^{(k)} = 0.006$, E-TPM still outperforms TPM by nearly 1000 times in terms of delay. Moreover, the right side in Fig. 6 indicates that the delay of TPM is over 80 000 times larger than that of E-TPM, whereas the power consumption of E-TPM is only 1.5 times larger than that of TPM. In other words, delay in TPM can be tremendously reduced by the proposed E-TPM at the cost of a slight more power consumption than TPM. Now, we explain the hills in Fig. 5. As $\rho^{(k)} = (\lambda_1^{(k)} + \lambda_2^{(k)})/\mu^{(k)}$ and $\mu^{(k)}$ is fixed to μ, increase in $\rho^{(k)}$ means $\lambda_1^{(k)} + \lambda_2^{(k)}$ grows, i.e., the amount of traffic increases. E-TPM consumes more energy and incurs less delay than TPM since the doze period of the former is probably shortened by an outgoing frame, whereas the latter is not. When

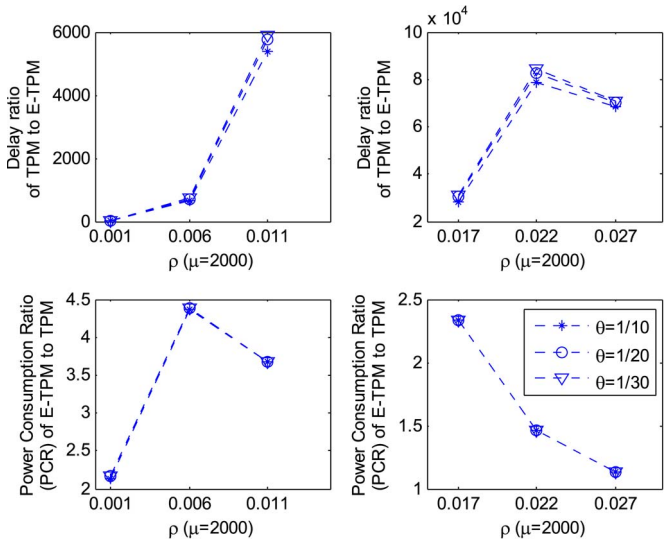

Fig. 6. Delay ratio and PCR (zoomed).

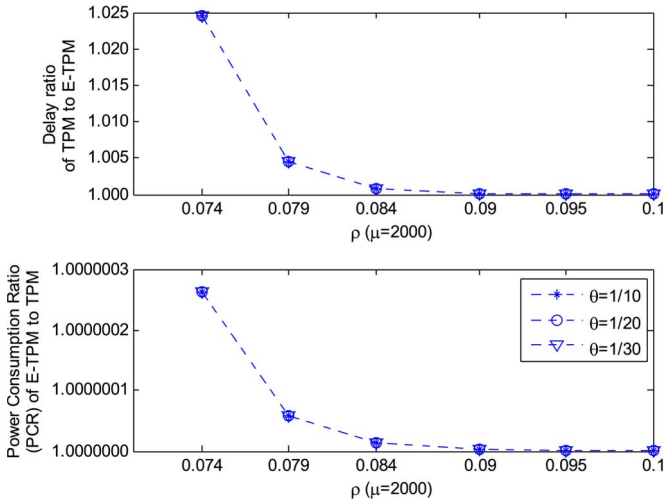

Fig. 7. Delay ratio and PCR versus ρ close to 0.1.

$\rho^{(k)}$ is small, the amount of traffic is small so that the STA under either TPM or E-TPM can enter the doze period to save energy. As $\rho^{(k)}$ grows, the doze period of E-TPM is frequently aborted by outgoing frames so that E-TPM consumes much more power than TPM, which increases PCR. As $\rho^{(k)}$ continues to grow, both schemes have no chance to sleep, which causes the power consumption of both schemes to gradually become close, thus reducing PCR. In other words, PCR exhibits up-and-down tendency such that the hill in PCR in Fig. 5 is formed. Now, we explain the hill in delay in Fig. 5. The main difference related to delay in E-TPM and TPM lies in outgoing frames. When $\rho^{(k)}$ is small, only a few outgoing frames are buffered in TPM such that the delays of both schemes are close. As $\rho^{(k)}$ increases, more outgoing frames are buffered in TPM, causing TPM to have more delay than E-TPM. When $\rho^{(k)}$ continues to grow, both schemes almost have no chance of sleeping so that their delays are close again, which generates the delay hill in Fig. 5.

In Fig. 5, for the $\rho^{(k)}$ value close to 0.1 (see the rightmost side in Fig. 5), both schemes seem to have the same delay ratio and PCR. To clearly observe the difference between them, we

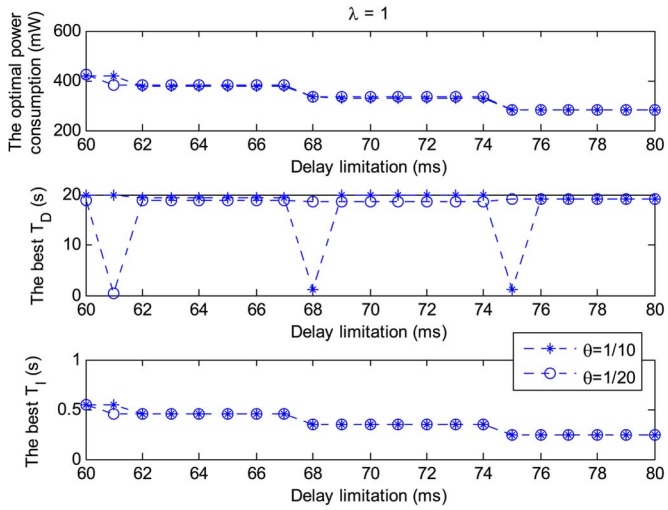

Fig. 8. Optimal power consumption versus delay limitation.

plot the rightmost part of Fig. 5 in Fig. 7. In Fig. 7, we observe that, even when the power consumption of the two schemes is very close, the proposed E-TPM still achieves delay better than TPM, which agrees with our intuition that E-TPM outperforms TPM in terms of delay. The reason is that each outgoing packet is transmitted right away under E-TPM, whereas it is kept in the buffer at the STA until the doze period of $T_D^{(k)}$ expires under TPM.

In some real-time applications, packets should be delivered to the destination within a given time period. Surely, packet delay is minimal if we let the STA stay awake all the time. However, it is not a good solution from the view of power saving. In fact, we can minimize the power consumption of the STA by allowing the STA to enter doze mode while keeping downlink packet delay within a given delay limitation, which can be formulated into the optimization problem shown in

$$\begin{aligned} \text{Min} \quad & E_{\text{avg}}^{(k)} \\ \text{w.r.t.} \quad & T_I^{(k)},\ T_D^{(k)} \\ \text{s.t.} \quad & T_{\text{Delay}}^{(k)} \le \overline{T};\quad \sum_{k=1}^{N} N_{\text{Buffer-ETPM}}^{(k)} \le \Gamma \\ & T_I^{(k)} = (m+0.5)BI, \qquad m = 1,2,\ldots,1000 \\ & T_D^{(k)} = jBI, \qquad j = 1,2,\ldots,3000 \end{aligned} \tag{30}$$

where $\overline{T}$ is the delay limitation, Γ is the limitation on the buffer size at the AP, and N is the number of nodes. We fix $N = 20$ in the following experiments.

First, we study the impact of the delay limitation $\overline{T}$ on power consumption without any limitation on the buffer size at the AP. Letting $\overline{T}$ vary from 60 to 80 ms, $\lambda = 1$, and setting $\theta^{(k)}$ to 1/10 and 1/20, we obtain the solution of the optimization problem in (30) as shown in Fig. 8, in which the optimal power consumption is shown in the top part, and its corresponding $T_D^{(k)}$ and $T_I^{(k)}$ are shown in the middle and bottom parts, respectively. In Fig. 8, we observe that, as the delay limitation $\overline{T}$ is relaxed (i.e., it grows), power consumption can be gradually decreased

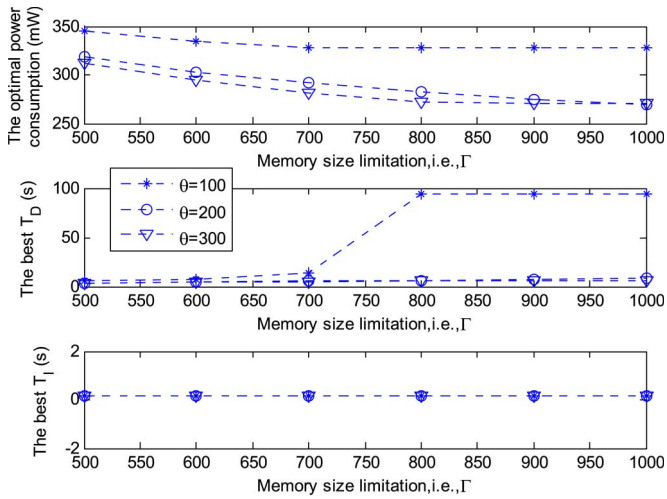

Fig. 9. Optimal power consumption versus memory limitation when $\overline{T} = 80$ ms.

by setting a suitable pair of parameters $T_D^{(k)}$ and $T_I^{(k)}$. For example, given $\theta^{(k)} = 1/10$, in the case where $\overline{T} = 61$ ms, we can obtain the optimal power consumption of 400 mW by setting $T_D^{(k)} = 20$ s and $T_I^{(k)} = 0.55$ s; in the case where $\overline{T} = 75$ ms, we can obtain the optimal power consumption of 300 mW by setting $T_D^{(k)} = 1$ s and $T_I^{(k)} = 0.35$ s.

Next, we study the impact of the memory size limitation Γ on power consumption. Clearly, in the case when $\theta^{(k)} < 1$, i.e., the uplink traffic is heavier than the downlink traffic, the dozing STA stops dozing frequently under E-TPM so that its frames buffered at the AP are received in short period of time, causing only a small size of memory to be enough for the buffered frames. Therefore, we consider the case $\theta^{(k)} > 1$. In particular, we set $\theta^{(k)} = 100$, 200, and 300. Letting Γ vary from 500 to 1000 frames, we achieve the solution of the optimization problem in (30) as shown in Fig. 9, from which we observe that power consumption can be gradually decreased (see the top part of the figure) by increasing the corresponding T_D (see the middle part of the figure) as memory size limitation Γ grows. In other words, we are able to decrease the power consumption by letting the STAs sleep longer when there is more available memory at the AP.

In summary, the proposed E-TPM, together with the optimization problem given in (30), is able to save energy with limited memory space at the AP and the preset delay bound for downlink packets.

VI. Conclusion

Power saving is a critical issue in the design of portable electronic devices. Considering that the existing power management schemes are not designed to support DIUT applications, we have proposed a power management scheme, namely, E-TPM for infrastructure IEEE 802.11 WLANs, in which two timers named the idle timer and the doze timer are included. E-TPM has the feature that the radio transceiver of the dozing STA is woken up right away when an outgoing frame is generated by the STA, regardless of whether the doze timer has expired or not. The proposed E-TPM significantly reduces delay compared with TPM [5] and can be used for DIUT applications. In E-TPM, energy consumption can be extremely reduced while packet delay can be controlled within a given time period by adjusting the values of the embedded pair of the idle and doze timers.

Appendix A

For the sake of concise description, we omit the superscript "(k)" used for the kth STA in this section. Given a pdf $h(x)$, its LST $h^*(s) = \int_0^\infty e^{-sx}h(x)dx$ satisfies

$$\int_0^\infty e^{-st}h'(t)dt = e^{-st}h(t)|_{t=0}^{t=\infty} + s\int_0^\infty h(t)e^{-st}dt$$
$$= s\cdot h^*(s) - h(0) \quad \text{(a.1)}$$
$$\lim_{t\to\infty} h(t) = \lim_{s\to 0} s\cdot h^*(s). \quad \text{(a.2)}$$

Applying the LST to t in (7) and (8), and using (16) and (a.1), we obtain

$$\left[\frac{d}{dx} + s + \lambda + \sigma(x)\right] p_{A_0}^*(s,x) = 0 \quad \text{(a.3)}$$
$$\left[\frac{d}{dx} + s + \lambda + \sigma(x)\right] p_{A_n}^*(s,x) = \lambda p_{A_{n-1}}^*(s,x)$$
$$n = 1, 2, \ldots \quad \text{(a.4)}$$

Solving (a.3) and (a.4), we obtain

$$p_{A_n}^*(s,x)$$
$$= \left[p_{A_0}^*(s,0)\frac{(\lambda x)^n}{n!} + p_{A_1}^*(s,0)\frac{(\lambda x)^{n-1}}{(n-1)!} + p_{A_2}^*(s,0)\frac{(\lambda x)^{n-2}}{(n-2)!}\right.$$
$$\left. + \cdots + p_{A_{n-1}}^*(s,0)\frac{\lambda x}{1!} + p_{A_n}^*(s,0)\right] e^{-(s+\lambda)x}\overline{F}(x)$$
$$(n = 0, 1, \ldots). \quad \text{(a.5)}$$

The correctness of (a.5) can be validated by directly substituting (a.5) into (a.3) and (a.4) (see [5] for the detailed derivation process of solving the differential (a.3) and (a.4)).

Similarly, applying the LST to t in (9) and (10) and using (14), we can obtain

$$p_{D_n}^*(s,x) = p_{D_0}^*(s,0)\frac{(\lambda_1 x)^n}{n!}e^{-(s+\lambda)x}\overline{G}(x) \qquad (n = 0, 1, \ldots). \quad \text{(a.6)}$$

Applying the LST in (15) and using (16), (a.1), and (a.5) leads to

$$[sP_I^*(s) - P_I(0)] + P_I^*(s)\frac{\lambda}{1-e^{-\lambda T_I}}$$
$$= \int_0^\infty p_{A_0}^*(s,x)\sigma(x)dx = \int_0^\infty p_{A_0}^*(s,0)e^{-(s+\lambda)x}\overline{F}(x)\sigma(x)dx$$
$$= p_{A_0}^*(s,0)\int_0^\infty e^{-(s+\lambda)x}f(x)dx = p_{A_0}^*(s,0)f^*(s+\lambda)$$

which is followed by

$$p^*_{A_0}(s,0)=\frac{1}{f^*(s+\lambda)}\left[\left(s+\frac{\lambda}{1-e^{-\lambda T_I}}\right)P^*_I(s)-1\right]. \quad \text{(a.7)}$$

Applying the LST in (13), and using (a.6) and (a.7), we have

$$\begin{aligned} p^*_{D_0}(s,0) &= P^*_I(s)\frac{\lambda e^{-\lambda T_I}}{1-e^{-\lambda T_I}}+\int_0^\infty p^*_{D_0}(s,x)\tau(x)dx \\ &= \left[1+p^*_{A_0}(s,0)f^*(s+\lambda)\right]\frac{\lambda e^{-\lambda T_I}}{s(1-e^{-\lambda T_I})+\lambda} \\ &\quad + p^*_{D_0}(s,0)g^*(s+\lambda) \end{aligned}$$

which yields

$$p^*_{D_0}(s,0)=\frac{\lambda e^{-\lambda T_I}P^*_I(s)}{[1-g^*(s+\lambda)]\,(1-e^{-\lambda T_I})}. \quad \text{(a.8)}$$

Applying the LST to t in (9) and (10) for $n=0,1,2,\ldots$ and then multiplying the derived equations with $z^n(n=0,1,2,\ldots)$, respectively, and summing all the derived equations, we obtain

$$\left[\frac{d}{dx}+s+\lambda+\tau(x)\right]Q^*(s,x,z)=\lambda_1 z Q^*(s,x,z)$$

which has the solution as follows after (9) is applied:

$$\begin{aligned} Q^*(s,x,z) &= Q^*(s,0,z)e^{-(s+\lambda-\lambda_1 z)x}\overline{G}(x) \\ &= p^*_{D_0}(s,0)e^{-(s+\lambda-\lambda_1 z)x}\overline{G}(x). \end{aligned} \quad \text{(a.9)}$$

Similarly, applying the LST to t in (7) and (8) for $n=0,1,2,\ldots$, then multiplying the derived equations with $z^n(n=0,1,2,\ldots)$, respectively, and summing all the derived equations, we can obtain

$$K^*(s,x,z)=K^*(s,0,z)e^{-(s+\lambda-\lambda z)x}\overline{F}(x). \quad \text{(a.10)}$$

Using (a.2), (a.9), and (a.8), we have

$$\begin{aligned} Q(z) &= \lim_{t\to\infty}\int_0^\infty Q(t,x,z)dx=\lim_{s\to 0}s\int_0^\infty Q^*(s,x,z)dx \\ &= \lim_{s\to 0}s\int_0^\infty P^*_{D_0}(s,0)e^{-(s+\lambda-\lambda_1 z)x}\overline{G}(x)dx \\ &= \lim_{s\to 0}sP^*_{D_0}(s,0)\overline{G}^*(s+\lambda-\lambda_1 z) \\ &= \lim_{s\to 0}s\frac{\lambda e^{-\lambda T_I}P^*_I(s)}{[1-g^*(s+\lambda)]\,(1-e^{-\lambda T_I})}\frac{1-g^*(s+\lambda-\lambda_1 z)}{s+\lambda-\lambda_1 z} \end{aligned}$$

followed by

$$Q(z)=P_I\frac{\lambda e^{-\lambda T_I}}{[1-g^*(\lambda)]\,(1-e^{-\lambda T_I})}\frac{1-g^*(\lambda-\lambda_1 z)}{\lambda-\lambda_1 z}. \quad \text{(a.11)}$$

Thus

$$P_D=\lim_{z\to 1}Q(z)=P_I\frac{\lambda e^{-\lambda T_I}}{[1-g^*(\lambda)]\,(1-e^{-\lambda T_I})}\frac{1-g^*(\lambda_2)}{\lambda_2}. \quad \text{(a.12)}$$

Now, we begin to derive $K^*(s,0,z)$. Applying the LST in (11) and (12) yields

$$\begin{aligned} p^*_{A_0}(s,0) &= \int_0^\infty p^*_{A_1}(s,x)\sigma(x)dx+\lambda P^*_I(s) \\ &\quad +\lambda_2\int_0^\infty p^*_{D_0}(s,x)dx+\int_0^\infty p^*_{D_1}(s,x)\tau(x)dx \\ p^*_{A_n}(s,0) &= \int_0^\infty p^*_{A_{n+1}}(s,x)\sigma(x)dx+\lambda_2\int_0^\infty p^*_{D_n}(s,x)dx \\ &\quad +\int_0^\infty p^*_{D_{n+1}}(s,x)\tau(x)dx, \qquad n=1,2,\ldots \end{aligned}$$

The above equations lead to

$$\begin{aligned} &K^*(s,0,z) \\ &= \sum_{n=0}^\infty p^*_{A_n}(s,0)z^n \\ &= \frac{1}{z}\left[\int_0^\infty K^*(s,x,z)\sigma(x)dx-\int_0^\infty p^*_{A_0}(s,x)\sigma(x)dx\right] \\ &\quad +\lambda P^*_I(s)+\lambda_2\int_0^\infty Q^*(s,x,z)dx \\ &\quad +\frac{1}{z}\left(\int_0^\infty Q^*(s,x,z)\tau(x)dx-\int_0^\infty p^*_{D_0}(s,x)\tau(x)dx\right). \end{aligned} \quad \text{(a.13)}$$

After using (a.5)–(a.10), the given equation can be recast as

$$\begin{aligned} &K^*(s,0,z) \\ &= \frac{1}{z-f^*(s+\lambda-\lambda z)} \\ &\quad \times\left\{1-P^*_I(s)\left\{s+\frac{\lambda}{1-e^{-\lambda T_I}}-\lambda z\right.\right. \\ &\qquad -\frac{\lambda e^{-\lambda T_I}}{[1-g^*(s+\lambda)]\,(1-e^{-\lambda T_I})} \\ &\qquad \times\left[\lambda_2 z\frac{1-g^*(s+\lambda-\lambda_1 z)}{s+\lambda-\lambda_1 z}\right. \\ &\qquad \left.\left.\left.+g^*(s+\lambda-\lambda_1 z)-g^*(s+\lambda)\right]\right\}\right\}. \end{aligned} \quad \text{(a.14)}$$

Using (a.10) and (a.14) leads to

$$\begin{aligned} K(z) &= \lim_{t\to\infty}\int_0^\infty K(t,x,z)dx=\lim_{s\to 0}s\int_0^\infty K^*(s,x,z)dx \\ &= \lim_{s\to 0}sK^*(s,0,z)\overline{F}^*(s+\lambda-\lambda z) \end{aligned}$$

$$
\begin{aligned}
&= \frac{\overline{F}^*(\lambda-\lambda z)P_I}{z-f^*(\lambda-\lambda z)} \\
&\quad \times \left\{ \frac{\lambda}{1-e^{-\lambda T_I}} + \lambda z + \frac{\lambda e^{-\lambda T_I}}{[1-g^*(\lambda)]\,(1-e^{-\lambda T_I})} \right. \\
&\qquad \left. \times \left[\lambda_2 z \frac{1-g^*(\lambda-\lambda_1 z)}{\lambda-\lambda_1 z} + g^*(\lambda-\lambda_1 z) - g^*(\lambda) \right] \right\} \\
&= P_I K_1(z) K_2(z) \qquad \text{(a.15)}
\end{aligned}
$$

where

$$
K_1(z) \equiv \frac{1-f^*(\lambda-\lambda z)}{z-f^*(\lambda-\lambda z)} \qquad \text{(a.16)}
$$

$$
\begin{aligned}
K_2(z) \equiv \frac{1}{1-z} \Bigg\{ & -\frac{1}{1-e^{-\lambda T_I}} + z + \frac{e^{-\lambda T_I}}{[1-g^*(\lambda)]\,(1-e^{-\lambda T_I})} \\
& \times \left[\lambda_2 z \frac{1-g^*(\lambda-\lambda_1 z)}{\lambda-\lambda_1 z} + g^*(\lambda-\lambda_1 z) - g^*(\lambda) \right] \Bigg\}.
\end{aligned} \qquad \text{(a.17)}
$$

It can be easily shown that

$$
\begin{cases}
\lim_{z\to 1} \frac{d}{dz} f^*(\lambda-\lambda z) = \lambda \int_0^\infty x f(x) dx = \lambda \mathrm{E}[\chi] = \frac{\lambda}{\mu} = \rho \\
\lim_{z\to 1} \frac{d^2}{dz^2} f^*(\lambda-\lambda z) = \lambda^2 \int_0^\infty x^2 f(x) dx = \lambda^2 \mathrm{E}[\chi^2] = \lambda^2.
\end{cases} \qquad \text{(a.18)}
$$

After introducing the notation $\zeta \equiv (d/dz) g^*(\lambda - \lambda_1 z)$, we obtain the following by applying L'Hôpital's rule on (a.17) and using (a.18)

$$
\lim_{z\to 1} K_1(z) = \frac{-\rho}{1-\rho} \qquad \text{(a.19)}
$$

$$
\lim_{z\to 1} K_2(z) = -\left[1 + \frac{\lambda}{\lambda_2} \frac{e^{-\lambda T_I}\,(1-g^*(\lambda_2))}{[1-g^*(\lambda)]\,(1-e^{-\lambda T_I})} \right]. \qquad \text{(a.20)}
$$

Using (a.15), (a.19), and (a.20), we obtain

$$
\begin{aligned}
P_A &= \lim_{z\to 1} K(z) = P_I \lim_{z\to 1} K_1(z) K_2(z) \\
&= P_I \frac{\rho}{1-\rho} \left[1 + \frac{\lambda}{\lambda_2} \frac{e^{-\lambda T_I}\,(1-g^*(\lambda_2))}{[1-g^*(\lambda)]\,(1-e^{-\lambda T_I})} \right]. \qquad \text{(a.21)}
\end{aligned}
$$

Noting $P_A + P_D + P_I = 1$ and using (a.12) and (a.21), we obtain

$$
P_I = (1-\rho) \left[1 + \frac{\lambda}{\lambda_2} \frac{e^{-\lambda T_I}\,(1-g^*(\lambda_2))}{[1-g^*(\lambda)]\,(1-e^{-\lambda T_I})} \right]^{-1}. \qquad \text{(a.22)}
$$

Substituting (a.22) into (a.21) leads to

$$
P_A = \rho. \qquad \text{(a.23)}
$$

In fact, (a.23) is the same as (17). In addition, (a.22) can be transformed into (18), and substituting (18) into (a.12) leads to (19), where the superscript "(k)" for the kth STA is put back.

APPENDIX B

As in Appendix A, we omit superscript "(k)." Clearly, (17)–(19) lead to (24) and (25). Moreover, using (a.16), (a.22), and L'Hôpital's rule, we obtain the following two equations:

$$
\lim_{z\to 1} \frac{d}{dz} K_1(z) = -\frac{\lambda^2 \beta}{2(1-\rho)^2} \qquad \text{(b.1)}
$$

$$
\lim_{z\to 1} \frac{d}{dz} K_2(z) = \frac{\lambda e^{-\lambda T_I}\,[\lambda_2 \zeta_1 - \lambda_1\,(1-g^*(\lambda_2))]}{(\lambda_2)^2\,[1-g^*(\lambda)]\,(1-e^{-\lambda T_I})} \qquad \text{(b.2)}
$$

where

$$
\begin{aligned}
\zeta_1 \equiv \lim_{z\to 1} \zeta &= \lim_{z\to 1} \frac{d}{dz} g^*(\lambda-\lambda_1 z) = \lambda_1 \int_0^\infty e^{-(\lambda-\lambda_1)x} x g(x) dx \\
&= \frac{\lambda_1 T_D}{2} e^{-2\lambda_2 T_D} + \frac{\lambda_1}{4\lambda_2} (1-e^{-2\lambda_2 T_D}). \qquad \text{(b.3)}
\end{aligned}
$$

Noting $N_{\text{Wait-ETPM}} = \sum_{n=1}^\infty n P_{A_n} = \lim_{z\to 1} d(K(z))/dz$ and using (23), (a.15), (a.16), and (b.1)–(b.3), we have (26).

As the average transmitting/receiving time of a frame is $1/\mu$, the waiting times of the first, second, …, $(N_{\text{Wait-ETPM}})$th are, respectively, $1/\mu, 2/\mu, \ldots$, and $N_{\text{Wait-ETPM}}/\mu$ such that the total waiting time of the $N_{\text{Wait-ETPM}}$ frames before they are transmitted/received is

$$
\begin{aligned}
T_{\text{Wait-ETPM}} &= 1/\mu + 2/\mu + \cdots + \lceil N_{\text{Wait-ETPM}} \rceil / \mu \\
&= \lceil N_{\text{Wait-ETPM}} \rceil \left(\lceil N_{\text{Wait-ETPM}} \rceil + 1 \right) / (2\mu)
\end{aligned}
$$

which is identical to (27). Using (18), (a.11), and (b.3), and noting $N^{(k)}_{\text{Bufferred-ETPM}} = \sum_{n=1}^\infty n P_{D_n} = \lim_{z\to 1} d(Q(z))/dz$, we achieve (28).

REFERENCES

[1] M. S. Gast, *802.11 Wireless Networks: The Definition Guide*. Sebastopol, CA, USA: O'Reilly, 2005.

[2] *IEEE 802.11 Standard—Wireless LAN Medium Access Control and Physical Layer Specifications*, IEEE Std. 802.11-2007, Jun. 2007.

[3] C. M. Chao, J.-P. Sheu, and I.-C. Chou, "An adaptive quorum-based energy conserving protocol for IEEE 802.11 ad hoc networks," *IEEE Trans. Mobile Comput.*, vol. 5, no. 5, pp. 560–570, May 2006.

[4] [Online]. Available: http://store.netgate.com/5004-MP-ATHEROS-4G-CM9-80211abg-miniPCI-Card-P125.aspx

[5] Y.-H. Zhu and V. C. M. Leung, "Efficient power management for infrastructure IEEE 802.11 WLANs," *IEEE Trans. Wireless Commun.*, vol. 9, no. 7, pp. 2196–2205, Jul. 2010.

[6] *IEEE 802.15.4 Standard for Wireless Medium Access Control (MAC) and Physical Layer (PHY) Specifications for Low-Rate Wireless Personal Area Networks (WPANs)*, IEEE Std. 802.15.4, 2011.

[7] S. Tozlu, "Feasibility of Wi-Fi enabled sensors for Internet of Things," in *Proc. 7th IWCMC*, 2011, pp. 291–296.

[8] S. Tozlu and M. Senel, "Battery lifetime performance of Wi-Fi enabled sensors," in *Proc. IEEE CCNC*, 2012, pp. 429–433.

[9] A. Berger, A. Potsch, and A. Springer, "Synchronized industrial wireless sensor network with IEEE 802.11 ad hoc data transmission," in *Proc. IEEE Int. Workshop M&N*, 2013, pp. 7–12.

[10] T. Zheng, R. Sridhar, and S. Venkatesh, "A switch agent for wireless sensor nodes with dual interfaces: Implementation and evaluation," *Tsinghua Sci. Technol.*, vol. 17, no. 5, pp. 586–598, Oct. 2013.

[11] Y.-C. Tseng, C.-S. Hsu, and T.-Y. Hsieh, "Power-saving protocols for IEEE 802.11-based multi-hop ad hoc networks," in *Proc. IEEE INFOCOM*, Jun. 2002, pp. 200–209.

[12] G. A. Safdar and W. G. Scanlon, "Performance analysis of an improved power-saving medium access protocol for IEEE 802.11 point coordination function WLAN," *IET Commun.*, vol. 153, no. 5, pp. 697–704, Oct. 2006.

[13] Y. He, R. Yuan, X. Ma, J. Li, and C. Wang, "Scheduled PSM for minimizing energy in wireless LANs," in *Proc. IEEE ICNP*, Oct. 16–19, 2007, pp. 154–163.
[14] K. M. Lau and O. C. Yue, "An improved IEEE 802.11 PSM based on server vacation models," in *Proc. IEEE 63rd VTC-Spring*, 2006, vol. 3, pp. 1256–1260.
[15] T.-C. Huang, J.-H. Tan, and C.-C. Huang, "A traffic-load oriented power saving mechanism for MAC protocol in ad hoc networks," in *Proc. IEEE WCNC*, Mar. 11–15, 2007, pp. 242–247.
[16] D. Ning *et al.*, "Realizing the full potential of PSM using proxying," in *Proc. IEEE INFOCOM*, 2012, pp. 2821–2825.
[17] R. Zheng, J. C. Hou, and L. Sha, "Performance analysis of power management policies in wireless networks," *IEEE Trans. Wireless Commun.*, vol. 5, no. 6, pp. 1351–1361, Jun. 2006.
[18] A. W. Min, R. Wang, J. Tsai, M. A. Ergin, and T.-Y. C. Tai, "Improving energy efficiency for mobile platforms by exploiting low-power sleep states," in *Proc. CF*, Cagliari, Italy, May 15–17, 2012, pp. 133–142.
[19] H. Tabrizi, G. Farhadi, and J. Cioffi, "An intelligent power save mode mechanism for IEEE 802.11 WLAN," in *Proc. IEEE GLOBECOM*, 2012, pp. 3460–3464.
[20] V. Miliotis, A. Apostolaras, T. Korakis, Z. Tao, and L. R. Tassiulas, "New channel allocation techniques for power efficient WiFi networks," in *Proc. IEEE 21st PIMRC*, 2010, pp. 347–351.
[21] J. Ma, S. H. Kim, and D. Kim, "Tame: Time window scheduling of wireless access points for maximum energy efficiency and high throughput," in *Proc. IEEE 18th RTCSA*, 2012, pp. 212–221.
[22] X. Chen, S. Jin, and D. Qiao, "M-PSM: Mobility-aware power save mode for IEEE 802.11 WLANs," in *Proc. 31st ICDCS*, 2011, pp. 77–86.
[23] Y.-H. Zhu, H. Lu, and V. C. M. Leung, "Access point buffer management for power saving in IEEE 802.11 WLANs," *IEEE Trans. Netw. Serv. Manag.*, vol. 9, no. 4, pp. 473–486, Dec. 2012.
[24] S. Wang, J. Y. Liu, J.-J. Chen, and X. Liu, "PowerSleep: A smart power-saving scheme with sleep for servers under response time constraint," *IEEE J. Emerging Sel. Topics Circuits Syst.*, vol. 1, no. 3, pp. 289–298, Sep. 2011.
[25] S. M. Ross, *Introduction to Probability Models (9th ed.)*. Singapore: Elsevier, 2007.
[26] Y. Rong, A. Y. Teymorian, L. Ma, X. Cheng, and H.-A. Choi, "A novel adaptation scheme for 802.11 networks," *IEEE Trans. Wireless Commun.*, vol. 8, no. 2, pp. 862–870, Feb. 2009.

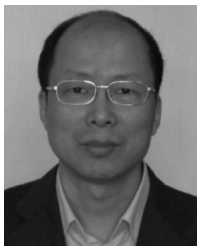

Yi-Hua Zhu (M'01–SM'07) received the B.S. degree in mathematics from Zhejiang Normal University, Zhejiang, China, in 1982; the M.S. degree in operation research and cybernetics from Shanghai University, Shanghai, China, in 1993; and the Ph.D. degree in computer science and technology from Zhejiang University, in 2003.

He is a Professor with Zhejiang University of Technology, Hangzhou, China. He has published more than 150 research papers in proceedings and journals, including the IEEE TRANSACTIONS ON WIRELESS COMMUNICATIONS and the IEEE TRANSACTIONS ON VEHICULAR TECHNOLOGY. His current research interests include information dissemination, stochastic modeling and analysis, power management, mobility management for wireless networks, and network coding.

Dr. Zhu is a member of the China Computer Federation Technical Committee on Sensor Networks. He has served as a Technical Program Committee Member in international conferences such as the IEEE International Conference on Communications, the IEEE Wireless Communications and Networking Conference, and the IEEE Global Communications Conference. He received the Best Paper Award from Chinacom in 2008.

Shenji Luan received the B.S. and M.S. degrees in communication engineering from Hangzhou Dianzi University, Zhejiang, China, in 2002 and 2005, respectively. He is currently working toward the Ph.D. degree in control science and enginering with Zhejiang University of Technology, Hangzhou, China.

He is currently with Hangzhou Dianzi University, Zhejiang. His current research interests include power management, energy conservation, and data communications for wireless networks, including wireless local area networks, wireless sensor networks, and cellular networks.

Victor C. M. Leung (S'75–M'89–SM'97–F'03) received the B.A.Sc. (Hons) degree in electrical engineering from the University of British Columbia (UBC), Vancouver, BC, Canada, in 1977, on a Natural Sciences and Engineering Research Council Postgraduate Scholarship, and the Ph.D. degree in electrical engineering in 1981.

From 1981 to 1987, he was a Senior Member of Technical Staff and a Satellite System Specialist with MPR Teltech Ltd., Canada. In 1988, he was a Lecturer with the Department of Electronics, Chinese University of Hong Kong, Shatin, Hong Kong. In 1989, he returned to UBC as a faculty member, where he is currently a Professor and the TELUS Mobility Research Chair in Advanced Telecommunications Engineering with the Department of Electrical and Computer Engineering. He has contributed to broad areas of wireless networks and mobile systems, in which he has coauthored more than 700 technical papers in international journals and conference proceedings and 27 book chapters and coedited six book titles. Several of his papers have been selected for best paper awards.

Dr. Leung is a Registered Professional Engineer in the Province of British Columbia, Canada. He is a Fellow of the Royal Society of Canada, the Engineering Institute of Canada, and the Canadian Academy of Engineering. He was a Distinguished Lecturer of the IEEE Communications Society. He is a member of the editorial board of the IEEE WIRELESS COMMUNICATIONS LETTERS, *Computer Communications*, and several other journals and has previously served on the editorial board of the IEEE JOURNAL ON SELECTED AREAS IN COMMUNICATIONS—Wireless Communications Series, the IEEE TRANSACTIONS ON WIRELESS COMMUNICATIONS, the IEEE TRANSACTIONS ON VEHICULAR TECHNOLOGY, the IEEE TRANSACTIONS ON COMPUTERS, and the *Journal of Communications and Networks*. He has guest edited many journal special issues and contributed to the organizing committees and technical program committees of numerous conferences and workshops. He was awarded the APEBC Gold Medal as the head of the graduating class in the Faculty of Applied Science. He received the IEEE Vancouver Section Centennial Award and the 2012 UBC Killam Research Prize.

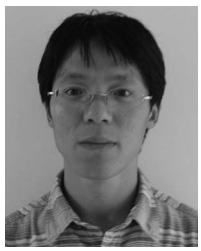

Kaikai Chi (M'11) received the B.S. and M.S. degrees from Xidian University, Xi'an, China, in 2002 and 2005, respectively, and the Ph.D. degree from Tohoku University, Sendai, Japan, in 2009.

From April 2009 to March 2010, he was a Postdoctoral Fellow with the Graduate School of Information Sciences, Tohoku University. He is currently an Associate Professor with the School of Computer Science and Technology, Zhejiang University of Technology, Hangzhou, China. He has published more than 30 refereed technical papers in proceedings and journals, including the IEEE TRANSACTIONS ON PARALLEL AND DISTRIBUTED SYSTEMS and the IEEE TRANSACTIONS ON VEHICULAR TECHNOLOGY. His current research focuses on wireless *ad hoc* networks and wireless sensor networks.

Dr. Chi received the Best Paper Award at the IEEE Wireless Communications and Networking Conference in 2008.